

# Inter-annual Variability of the Current System off the West Greenland Coast from a very high-resolution numerical model

Ruijian Gou<sup>1</sup>, Clark Pennelly<sup>2</sup>, and Paul G. Myers<sup>2</sup>

<sup>1</sup>Key Laboratory of Physical Oceanography and Frontiers Science Center for Deep Ocean Multispheres and Earth System, Ocean University of China

<sup>2</sup>University of Alberta

November 23, 2022

## Abstract

Analyzing a high-resolution ( $1/60^\circ$ ) numerical model over 2008 to 2018, the inter-annual variability of the West Greenland Coastal Current (WGCC) on the shelf and West Greenland Current (WGC) at shelf break is presented. Both currents flow from Cape Farewell and extend to Davis Strait, with their model speeds and transports corresponding well with observations. The inter-annual variability of the WGCC and WGC near southwest Greenland are opposite, with the former declining while the latter strengthened, both by a speed change above 0.1 m/s. Both currents are predominantly buoyancy forced, but wind forcing becomes more dominant towards Davis Strait. The main exchanges from the two currents to interior occur between Cape Desolation and Fylla Bank, with net volume, freshwater, heat transport decreases of 1.4 Sv, 13 mSv, 36.7 TW. The freshwater transport of the WGC itself does not drop in between these sections, receiving freshwater from the WGCC to compensate for the losses to the basin interior. Thus, we see significant freshwater (83.1 mSv) and heat transports (70.7 TW) of the WGC remaining at Fylla Bank that reach the northern basin instead of being fluxed into the interior of the Labrador Sea. This suggests that the exchange between the current system and the interior is more limited than previously thought, and most of the Greenland and Arctic melt reaches the northern Labrador Sea. Our results highlight the importance of resolving the WGCC and shelf processes.

1 **Inter-annual Variability of the Current System off the West Greenland Coast from a**  
2 **very high-resolution numerical model**

3 **Enter authors here: Ruijian Gou<sup>1,2</sup>, Clark Pennelly<sup>2</sup> and Paul G. Myers**

4 <sup>1</sup>Key Laboratory of Physical Oceanography and Frontiers Science Center for Deep Ocean  
5 Multispheres and Earth System, Ocean University of China, Qingdao, China

6 <sup>2</sup>Department of Earth and Atmospheric Sciences, University of Alberta, Edmonton, Alberta,  
7 Canada.

8 Corresponding author: Paul G. Myers (<mailto:pmyers@ualberta.ca> )  
9

10 **Key Points:**

- 11 • The net freshwater transport of the WGC does not drop between Cape Desolation and  
12 Fylla Bank sections
- 13 • Along southwest Greenland, the shelf component weakens while the shelf break  
14 component strengthens, both by  $>0.1 \text{ m s}^{-1}$ , over 2008-2018.
- 15 • The current system is buoyancy driven near southwest Greenland, with wind forcing  
16 more dominant in the north.

17 **Abstract**

18 Analyzing a high-resolution ( $1/60^\circ$ ) numerical model over 2008 to 2018, the inter-annual  
19 variability of the West Greenland Coastal Current (WGCC) on the shelf and West Greenland  
20 Current (WGC) at shelf break is presented. Both currents flow from Cape Farewell and extend to  
21 Davis Strait, with their model speeds and transports corresponding well with observations. The  
22 inter-annual variability of the WGCC and WGC near southwest Greenland are opposite, with the  
23 former declining while the latter strengthened, both by a speed change above 0.1 m/s. Both  
24 currents are predominantly buoyancy forced, but wind forcing becomes more dominant towards  
25 Davis Strait. The main exchanges from the two currents to interior occur between Cape  
26 Desolation and Fylla Bank, with net volume, freshwater, heat transport decreases of 1.4 Sv, 13  
27 mSv, 36.7 TW. The freshwater transport of the WGC itself does not drop in between these  
28 sections, receiving freshwater from the WGCC to compensate for the losses to the basin interior.  
29 Thus, we see significant freshwater (83.1 mSv) and heat transports (70.7 TW) of the WGC  
30 remaining at Fylla Bank that reach the northern basin instead of being fluxed into the interior of  
31 the Labrador Sea. This suggests that the exchange between the current system and the interior is  
32 more limited than previously thought, and most of the Greenland and Arctic melt reaches the  
33 northern Labrador Sea. Our results highlight the importance of resolving the WGCC and shelf  
34 processes.

35 **Plain Language Summary**

36 The West Greenland Coastal Current (WGCC) is a shelf current that carries the cold and fresh  
37 water from the Arctic and Greenland, and the West Greenland Current (WGC) is a shelf break  
38 current that carries the Arctic water at surface and warm, salty Atlantic water at depth. Their  
39 transports could have a significant impact on the stratification in the Labrador Sea. However, due

40 to the lack of observations and insufficient model resolution, their inter-annual variability is not  
41 understood yet. In this study, we present their inter-annual variability along the west Greenland  
42 coast, from a high-resolution numerical model from 2008 to 2018. Both currents flow from  
43 Cape Farewell north to Davis Strait. The variability of the WGCC and WGC near southwest  
44 Greenland are opposite, with the former declining while the latter strengthened. The currents are  
45 forced by both wind and buoyancy, with wind more important the further north. Between Cape  
46 Desolation and Fylla Bank is where the most offshore exchanges from the currents to the interior  
47 Labrador Sea occurs. Nevertheless, the exchanges are limited as the majority of the freshwater  
48 and heat flows to the north.

## 49 **1 Introduction**

### 50 1.1 West Greenland Current

51 The West Greenland Current (WGC; Figure 1) has a significant role in modulating the  
52 deep convection in the Labrador Sea (Li et al., 2021), where an important mode water –  
53 Labrador Sea Water (LSW), is produced. It is a strong current that is situated on the shelf break  
54 of west Greenland. It carries a significant amount of buoyant water, with low salinity water of  
55 Arctic origin at the surface, as well as the warm and salty Irminger water at intermediate depths  
56 (Myers et al., 2007; Frattoni and Pickart, 2007; Pacini et al., 2021). These water masses are  
57 transported into the interior Labrador Sea either through offshore Ekman transport (e.g., Luo et  
58 al., 2016; Schulze-Chretien & Frajka-Williams, 2018) or eddies (e.g., Bracco et al., 2008; de  
59 Jong et al., 2014; Katsman et al., 2004). This lateral exchange offers a buoyancy flux to restratify  
60 the water column (Luo et al., 2016), thus affecting the deep convection. Therefore, the WGC's  
61 volume/freshwater transport can significantly modulate the density anomaly across the Labrador  
62 Sea (Zou et al., 2020) impacting convection, LSW formation and potentially the Atlantic  
63 Meridional Overturning Circulation (AMOC; Li et al., 2021).

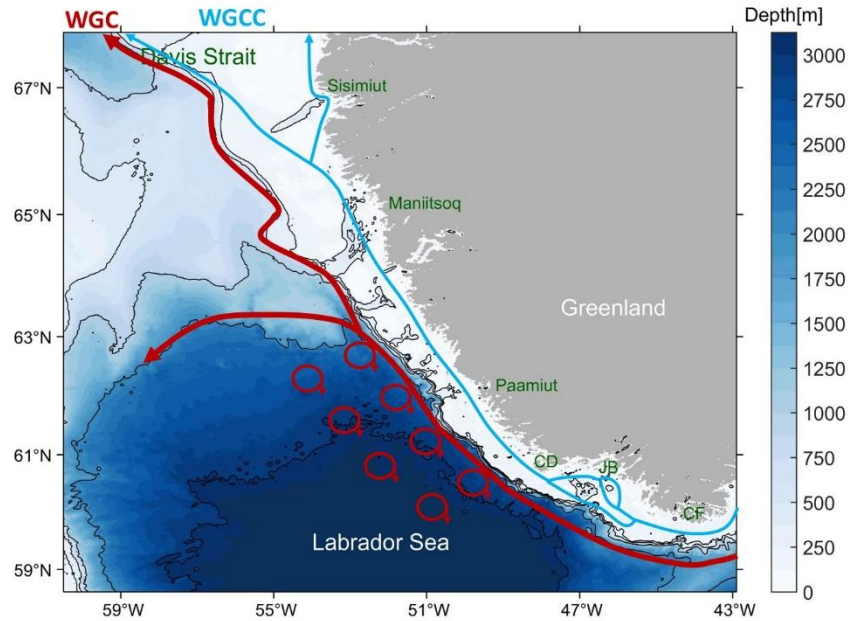
64 In terms of the WGC transports, Myers et al. (2009) calculated a mean summer volume  
65 transport (relative to the 34.8 isohaline and 700 db) for 1984-2005 of  $5.5 \pm 3.9$  Sv at the Cape  
66 Desolation section that decreases northward to  $0.0 \pm 0.3$  Sv at the Sisimiut section, using the  
67 data from the Greenland Institute of Natural Resources (GINR) standard sections (Figure 2;  
68 Mortensen, 2018). The corresponding mean freshwater transports, referenced to a salinity of 34.8  
69 are  $54.4 \pm 22.4$  mSv at Cape Desolation section and  $0.03 \pm 5.4$  mSv at Sisimiut section. Using  
70 multiple hydrography datasets for 1992-2008, Rykova et al. (2015) showed a mean volume  
71 transport (relative to the 3000 m isobath, 34.4 isohaline and 1000 db) of  $1.8 \pm 0.15$  Sv and a  
72 mean freshwater transport of  $60.1 \pm 16$  mSv (referenced to a salinity of 34.3) at the AR7W  
73 section. Besides those observational studies, a study using an eddy-permitting model showed that  
74 the mean northward components of the volume transport and freshwater transport referenced to a  
75 salinity of 34.8 for 1965-2002 across the Davis Strait are 1.2 Sv and 15.7 mSv respectively  
76 (Lique et al., 2009), despite the net transport at Davis Strait being southward (Curry et al., 2011,  
77 2014). An eddy-rich modelling study revealed that the mean WGC volume transports for 2004-  
78 2013 at Maniitsoq and Sisimiut are  $\sim 0.8$  Sv and  $\sim 0.7$  Sv respectively, and the corresponding  
79 mean WGC heat transports referenced to  $0^\circ\text{C}$  are  $\sim 10$  TW for each section (Myers et al., 2021).  
80 However, the transport comparison among the studies is difficult considering the different time  
81 periods and definitions for the currents.

82 1.2 West Greenland Coastal Current

83 As a part of the West Greenland Current system, the West Greenland Coastal Current  
84 (WGCC; Figure 1), a recently discovered shelf current (Lin et al., 2018), has recently received  
85 attention since it carries the coldest and freshest water in this region, the upper polar water  
86 (Pacini et al., 2020). It was found that the East Greenland Coastal Current (EGCC), located on the  
87 east Greenland shelf, keeps its identity rounding Cape Farewell (Lin et al., 2018; Pacini et al.,  
88 2020), becoming the WGCC. That said, the WGCC is distinguished from the EGCC as its  
89 boundary with the shelf break current is not as clear (Duryck et al., 2021; Gou et al., 2021).  
90 Furthermore, it has been suggested that there may be considerable exchange between the WGCC  
91 and the WGC near Cape Farewell (Lin et al., 2018; Gou et al., 2021).

92 The WGCC was first demonstrated in the analysis of a summer cruise survey data in  
93 2014 (Lin et al., 2018). They showed that as it goes from Cape Farewell to Cape Desolation, its  
94 volume transport and freshwater transport decrease from 1.01 Sv to 0.42 Sv and from 49.50 mSv  
95 to 23.32 mSv, respectively (referenced to 34.8). Recently, its seasonality was studied by the  
96 sectional data from the Overturning in the Subpolar North Atlantic Program (OSNAP; Lozier et  
97 al., 2017) (Pacini et al., 2020) and combined in situ and satellite data (Majumder et al., 2021).  
98 Additionally, a recent high-resolution modelling study (Gou et al., 2021) has revealed very  
99 similar seasonal features as these observations showed, such as the seasonal transport cycles.

100 Nevertheless, the inter-annual variability of the WGCC and WGC remain largely  
101 unknown, considering the short time-span (2014-2018) of the OSNAP data and the mainly  
102 summertime occupations of the other sections. Additionally, the fate of the WGCC north of Cape  
103 Desolation is an open question. Thus our use of a very high-resolution numerical model provides  
104 an useful tool for studying the behavior of the WGC/WGCC system along the west Greenland  
105 coast, including the system's inter-annual variability. Given its ability to resolve the Rossby  
106 radius and many mesoscale features with a resolution reaching 800 m, the model is able to  
107 represent realistic behavior on the shelf (e.g. Pennelly and Myers, 2021, Gou et al., 2021), as  
108 well as the offshore exchange into the Labrador Sea (e.g. Pennelly and Myers, 2021). Thus, we  
109 use a decade of output of our model to study the inter-annual variability of the WGCC and  
110 WGC, analyzing the currents and their speed, transports and forcings, as well as the exchange  
111 into the Labrador Sea.



112

113 **Figure 1.** Schematic showing the geographical features and mean circulation pathways off the  
 114 west Greenland coast. The blue and red arrows correspond to the WGCC and WGC respectively,  
 115 and the red circles denote eddies shed by the WGC. CF, JB, CD, denotes Cape Farewell,  
 116 Julianehaab Bight, Cape Desolation respectively. The black contour lines indicate the 250, 500,  
 117 1,000, 2,000, and 3,000 m isobaths and the contour interval is non-linear.

## 118 2 Model and Method Description

### 119 2.1 Model

120 The model used in this study is based on the NEMO numerical framework, version 3.6  
 121 (Madec, 2008). It has an inner nest of  $1/60^\circ$  resolution in the Labrador Sea, with a couple of  
 122 outer nests covering the Arctic and the North Hemisphere Atlantic (ANHA; Hu et al., 2018) and  
 123 the sub-polar gyre (Pennelly and Myers, 2020). In our study area, the horizontal resolution is  
 124 around 800~1100 m. Thus only within this nest can the model resolves the first baroclinic  
 125 Rossby radius on the shelf (Gou et al., 2021). The atmospheric forcing has been changed to  
 126 Drakkar Forcing Set 5.2 (DFS5.2; Dussin et al., 2016), instead of the Canadian Meteorological  
 127 Centre's Global Deterministic Prediction System ReForecast product (CGRF; Smith et al., 2014)  
 128 used in Gou et al. (2021), to better represent convection in the Labrador Sea (Pennelly and  
 129 Myers, 2021). Ten-years of output from 2008 to 2018 saved as daily averages are used in this  
 130 study. The vertical mesh consists of 75 layers with  $\sim 1$  m resolution at the surface that decreases  
 131 with depth, and the top 250 m is made up by 34 layers. The implementation of the simulation,  
 132 the initial and boundary conditions, and other forcings, are explained in Gou et al. (2021). For  
 133 further details of the model setup, please refer to Pennelly and Myers (2020).

### 134 2.2 Transport calculation

135 We look into the current transports at eight observational sections (Figure 2): OSNAP  
 136 West (Lozier et al., 2017), the Greenland Institute of Natural Resources (GINR) standard

137 sections – Cape Farewell, Cape Desolation, Fylla Bank, Maniitsoq, Sisimiut (Mortensen, 2018),  
 138 and the regularly sampled WOCE AR7W line (Hall et al., 2013). We extend the sections onshore  
 139 to cover the coastal current, and extend the northern three sections offshore to cover the whole  
 140 WGC (Figure 2).

141 The transports are defined to be positive when they are directed to the north and  
 142 northwest along the main axis of the west Greenland shelf. The WGCC transports are based on  
 143 integrating the model velocity fields perpendicular to each section where the bathymetry is  
 144 shallower than 250m (see Figure 1) and WGC transports are based on integrating farther offshore  
 145 where the speed is larger than 0.1 m/s and the salinity is smaller than 34.8. Focusing on the  
 146 freshwater component of the WGC instead of its Irminger water component, we thus apply the  
 147 34.8 isohaline to denote the edge of the WGC as Myers et al. (2009) did. Since eddies are  
 148 generated and shed by the WGC between Cape Desolation and Fylla Bank, for these sections, the  
 149 WGC transport integrals are defined to only include those grid points where the velocity  
 150 direction is northward along the coast. Since the speed of the WGC begins to slow at Maniitsoq  
 151 and Sisimiut, and the offshore parts of the sections may capture the southward flow near the  
 152 western boundary, for these sections, the definition for the WGC transport is changed to  
 153 integrating offshore from the WGCC to where the salinity is smaller than 34.8 and the velocity  
 154 direction is northward along the coast. We calculate the freshwater transports and heat transports  
 155 based on multiple reference values, due to the variety of them used in different studies (Gou et  
 156 al., 2021). We only present the results referenced to 34.8 salinity and -1.8°C temperature in this  
 157 manuscript, with the results referenced to other values in the supplementary material (Figures  
 158 S1-S4).

### 159 2.3 Method for analyzing the forcing mechanisms

160 We apply the method from Whitney and Garvine (2005) that computes the wind-forced  
 161 velocity components ( $u_w$ ) and buoyancy-forced velocity components ( $u_b$ ) of the currents.  $u_w$  is  
 162 induced by the wind-forced sea surface height gradient and  $u_b$  is induced by the horizontal  
 163 density gradient. The wind strength index ( $W_s$ ), the ratio between the  $u_w$  and  $u_b$ , denotes the  
 164 relative importance between wind and buoyancy forcing. When  $|W_s|$  is  $>1$ , the current is  
 165 predominantly wind-driven. And when  $|W_s|$  is  $<1$ , the current is predominantly buoyancy-driven.

166 This method has been applied to the EGCC, using observations (Sutherland & Pickart,  
 167 2009) and modelling (Bacon et al., 2014). And it has been applied in the observational study of  
 168 the WGCC by Lin et al. (2018). Here, we follow the application of this method by Bacon et al.  
 169 (2014) as our study also uses a numerical model.

170 The wind-forced velocity component  $u_w$  is defined as

$$171 \quad u_w = \sqrt{\frac{\rho_{air} C_{10}}{\rho C_D}} \cdot U$$

172 where  $\rho_{air}$  is air density set as a constant of 1.293 kg/m<sup>3</sup>,  $\rho$  is water density set as a constant of  
 173 10<sup>3</sup> kg/m<sup>3</sup>,  $C_{10} = 10^{-3} \left( \frac{2.7}{|U|} + 0.142 + \frac{|U|}{13.09} \right)$  is the surface drag coefficient,  $C_D$  is the bottom drag  
 174 coefficient set as a constant of 10<sup>-3</sup>, and  $U$  is the along-shelf 10-m wind speed (the component  
 175 normal to the section) from DFS5.2 over the period of 2008-2017.  $U$  is averaged over the

176 coordinate points comprising each section that covers the width of each current, and  $|U|$  is its  
177 absolute value.

178 The buoyancy-forced velocity component  $u_b$  is defined as

$$179 \quad u_b = \frac{R_1}{W} (2g'Qf)^{1/4}$$

180 where  $R_1$  is the first baroclinic Rossby radius,  $W$  is the width of the current,  $g'$  is the reduced  
181 gravity,  $Q$  is the volume transport of the current, and  $f$  is the Coriolis parameter set as a constant  
182 of  $1.3 \times 10^{-4} \text{ s}^{-1}$ . Specifically,  $R_1 = NH/f\pi$  is calculated at the location of the maximum of the top-  
183 250 m averaged speed, where  $H$  denotes the full water depth for the WGCC or the depth where  
184 the salinity is below 34.8 for the WGC.  $N^2 = -\left(\frac{g}{\rho}\right) \frac{\partial \rho}{\partial z}$  is the buoyancy frequency and  $\frac{\partial \rho}{\partial z}$  is  
185 estimated as the density difference between the surface layer and the layer with a depth of  $H$ ,  
186 divided by  $H$  (i.e.  $\Delta z$ ).  $W$  is the distance between the points where the speed falls to 70% of  
187 the maximum. The densities at those points are used to estimate  $g' = g(\rho_2 - \rho_1)/\rho_1$ , where  $g$  is set to  
188 be  $9.8 \text{ m s}^{-2}$  and  $\rho_2$  is on the offshore side. These densities are computed at 75 m depth, except at  
189 Fylla Bank and Sisimiut, where the surface layer is used as the continental shelf of these two  
190 sections are very shallow. Note that at the Fylla Bank and Sisimiut sections, as the currents are  
191 not coherent, and do not have a clear core that their speeds decline away from. Thus, to define  
192  $W$ , the currents were divided into several branches when calculating  $W$ . So for these two  
193 sections,  $W$  and corresponding  $g'$  are the sum of the  $W$  and  $g'$  of each branch. To avoid the  
194 southward flow in the west Labrador Sea at Sisimiut, only the offshore 180 km of the section are  
195 included in the calculation for that section.

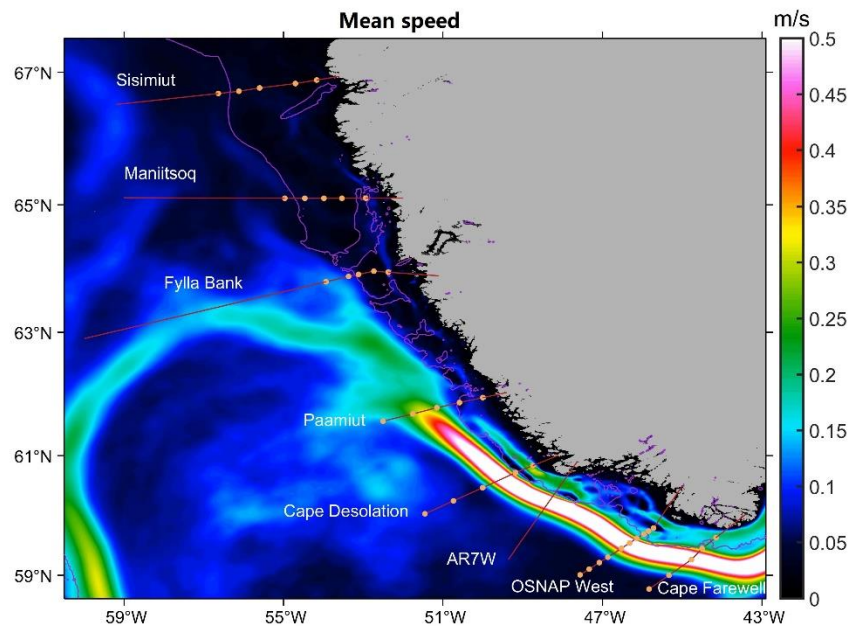
### 196 **3 Speeds**

#### 197 **3.1 Annual mean structure**

198 We first look at the top-50 m model annual mean speed field off the west Greenland  
199 coast, averaged over 2008-2018 (Figure 2). The WGCC remains coherent with a strong year-  
200 round on-shelf jet from the Cape Desolation section almost to the Paamiut section. Significant  
201 flow remains on the shelf north to the Sisimiut section and Davis Strait. Bands of narrow flow  
202 with annual mean velocities exceeding  $0.1 \text{ m s}^{-1}$  can be seen in the deeper water inshore of the  
203 various banks interspaced with regions of broader and weaker flow, consistent with the observed  
204 shelf flow around the Fylla Bank section (Myers et al., 2009). In the annual mean, the flow  
205 separates on the shelf between the Maniitsoq and Sisimiut sections, with most of the flow  
206 moving towards the shelf-break as the Sisimiut section is approached. The mean velocities  
207 inshore of the Maniitsoq section are close to  $0.1 \text{ m s}^{-1}$ , and those at the Sisimiut section are  
208 generally lower than  $0.05 \text{ m s}^{-1}$ , same as indicated by Myers et al. (2009). For further  
209 comparison, a direct measurement of the northward surface velocity on the west Greenland  
210 shelf across the Davis Strait is  $0.06 \text{ m s}^{-1}$  while an estimate using hydrographic data is  $0.02 \text{ m s}^{-1}$   
211 (Azetsu-Scott et al, 2011). And the shelf velocity was observed to reach  $0.1 \text{ m s}^{-1}$  during 1987-  
212 1990 (Cuny et al., 2005).

213 The WGC continues north as a strong current with annual mean core velocities exceeding  
214  $0.5 \text{ m s}^{-1}$  until the Paamiut section, where there is a broad region with velocities exceeding  $0.2 \text{ m s}^{-1}$   
215  $\text{s}^{-1}$ . Northward to the Fylla Bank section, the continental slope gets flatter as the 2000m and  
216 3000 m isobaths veer westward sharply. Correspondingly, the WGC splits into two branches at

217 the Fylla Bank section, with the major one along the 2000 m isobath, eventually joining the  
 218 Labrador Current with velocities reaching  $0.2 \text{ m s}^{-1}$ , and a narrower, weaker branch heading  
 219 northward to Davis Strait and into Baffin Bay. Considering the fact that currents follow the  $f/H$   
 220 contours ( $f$  denotes Coriolis parameter and  $H$  denotes the bottom depth), the mean path of the  
 221 northward branch largely follows the curving 500 m isobath close to the west Greenland shelf  
 222 break, thus interacting with the observed southward flows that veer eastward from the western  
 223 strait (Cuny et al., 2005; Curry et al., 2011; Curry et al., 2014). These phenomenon in the model  
 224 also correspond to what was found in the observational study by Myers et al. (2009). And the  
 225 paths of the WGCC and WGC from the Cape Farewell section to Davis Strait were similarly  
 226 illustrated by Curry et al. (2014). The annual speeds of this northward branch could be as low as  
 227 below  $0.05 \text{ m s}^{-1}$ , and as high as above  $0.15 \text{ m s}^{-1}$ . Stein (2004) had estimated that the speed of  
 228 the WGC flowing through the Davis Strait is in the range of  $0.1\text{-}0.36 \text{ m s}^{-1}$ . The modelling study  
 229 by Lique et al. (2009) suggested that the WGC speed across the Davis Strait could reach  $0.1 \text{ m s}^{-1}$ .  
 230 And a recent observational study by Majumder et al. (2021) has shown that the speed of the  
 231 WGC flowing from  $61^\circ\text{N}$  to  $64\text{-}65^\circ\text{N}$  is approximately  $0.17 \text{ m s}^{-1}$ .

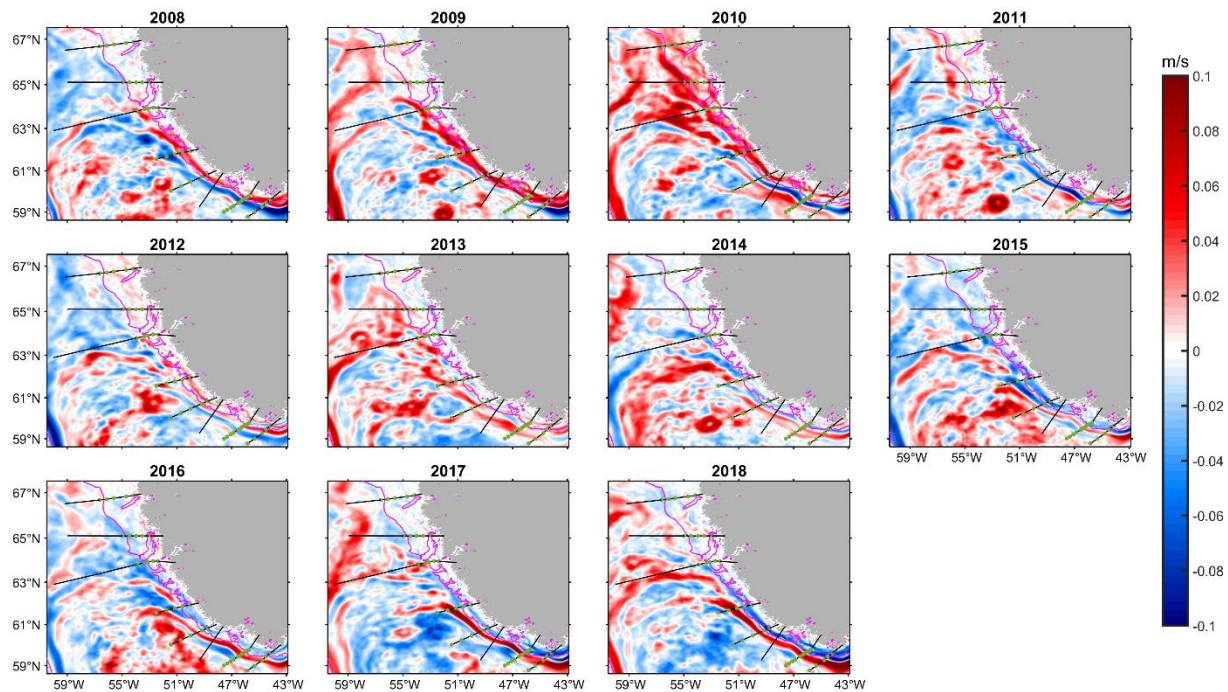


232  
 233 **Figure 2.** Mean model top-50m speed field off the west Greenland coast for 2008-2018. Sections  
 234 are shown by red lines, with yellow dots representing the actual stations, and the purple lines  
 235 denote the 250m isobath.

### 236 3.2 Inter-annual variability

237 It is noted that north of Fylla Bank in 2010, the WGC and WGCC have speeds of  $\sim 0.15$   
 238  $\text{m s}^{-1}$  and  $\sim 0.1 \text{ m s}^{-1}$  respectively (Figure S5), which are the highest in the ten-year period. This  
 239 anomaly is also reflected in Figure 3 revealing the annual anomaly, showing that the speed  
 240 increases of the northern WGCC and WGC reached  $\sim 0.05 \text{ m s}^{-1}$  and  $\sim 0.1 \text{ m s}^{-1}$  respectively, that  
 241 year. This is related to anomalously large northward Ekman transport, increasing the transport of the WGC north  
 242 through Davis Strait (Myers et al., 2021).  
 243

244 It is seen from Figure 3 that, south of Fylla Bank section, the speed anomaly of the  
 245 WGCC becomes negative in the later years, while the negative speed anomaly of the WGC  
 246 turns to positive correspondingly. Therefore, the inter-annual trend of the WGCC speed is opposite to  
 247 that of the WGC over 2008-2018. The WGCC weakens by more than  $0.1 \text{ m s}^{-1}$  as the WGC  
 248 strengthens with a speed increase that approaches  $0.2 \text{ m s}^{-1}$ . This relation is especially noticeable  
 249 south of Paamiut section, where the WGC is stable and does not shed eddies. North of Fylla  
 250 Bank section, for both currents, the general speed anomaly does not follow the same pattern,  
 251 both in terms of the magnitude and inter-annual variations. For example in 2010, there is a large  
 252 positive speed anomaly for the northern WGC but large negative speed anomaly to the south.  
 253 Furthermore, the difference between the north and south implies that the forcing mechanisms of  
 254 the currents north of Fylla Bank section may be different from those to the south.



255 **Figure 3.** Annual anomalies of the top-50m speed field for the given years referenced to the  
 256 2008-2018 mean. Sections are shown by black lines, with green dots representing the actual  
 257 stations, and the magenta lines denote the 250m isobath.  
 258

259

## 260 4 Transports

### 261 4.1 Annual mean transports

262 The time-mean transports of the WGCC are presented in Figure 4. In comparison with  
 263 the same model driven by different atmospheric forcing (see Table 1 in Gou et al. (2021)),  
 264 differences are larger to the south, with the volume transport at Cape Farewell section being  
 265  $0.14 \text{ Sv}$  smaller and  $0.07 \text{ Sv}$  smaller at the OSNAP West section. For the AR7W and Cape  
 266 Desolation sections, the differences are negligible. The model sensitivity to the atmospheric  
 267 forcing is strongest near Cape Farewell and maybe related to the inflows into the inner nest. Our  
 268 time-mean volume transports of the WGC for 2008-2018 (Figure 4a) are in the ranges of the

269 means for 1984-2005 shown by Myers et al. (2009), except for larger values at Fylla Bank (3.5  
270 Sv versus  $1.1 \pm 0.9$  Sv) and Maniitsoq (1.2 Sv versus  $0.1 \pm 0.2$  Sv). This could be due to the fact  
271 that we include the unstable part of the WGC that sheds eddies at Fylla Bank, and a part of the  
272 WGC at Maniitsoq is located in the extended part of the section in this analysis.

273 Our time-mean freshwater transports are generally larger than Myers et al. (2009)'s  
274 results (e. g., 81.9 mSv versus  $45.8 \pm 11.8$  mSv at Cape Farewell, 84.3 mSv versus  $47.7 \pm 12.3$   
275 mSv at Paamiut, and 12.2 mSv versus  $0.03 \pm 5.4$  mSv at Sisimiut) with the differences smallest  
276 at the Cape Desolation section (78.0 mSv vs  $54.4 \pm 22.4$  mSv). A speculation for the larger  
277 transports seen in this study is that the subarctic has undergone notable freshening, consistent  
278 with Arctic and Greenland warming and melting (Dukhovskoy et al., 2019). Additionally it may  
279 be that the Myers et al. (2009) values were biased low because of a poor representation of the  
280 low salinity flows on the shelf. In terms of mean heat transports referenced to  $0^\circ\text{C}$  (Figure S4),  
281 other than the differently defined Fylla Bank and Maniitsoq sections, our results are generally in  
282 the ranges of those presented by Myers et al. (2009). The exception is the Paamiut section where  
283 our heat transport of greater than 60 TW is much larger than the previous estimate of  $25 \pm 13$   
284 TW.

285 For both the WGCC and WGC at the Sisimiut section, the combined model mean volume  
286 transport (0.45 Sv) and freshwater transport (16.4 mSv) (Figure 4) are very close to the Davis  
287 Strait transport estimates from previous observational studies, despite different definitions for the  
288 transport integrals. For instance, Curry et al. (2011) showed that the mean volume and freshwater  
289 transport (referenced to a salinity of 34.8) for the west Greenland shelf for 2004-2005 are 0.4 Sv  
290 and 15 mSv respectively. Another study by Curry et al. (2014) found that the mean volume and  
291 freshwater transport (referenced to a salinity of 34.8) of the West Greenland Shelf Water  
292 (recognized as the WGC; potential temperature  $< 7^\circ\text{C}$ ; salinity  $< 34.1$ ) for 2004-2010 was 0.4 Sv  
293 and 17 mSv respectively. Their heat transport (referenced to  $0^\circ\text{C}$ ) was computed to be 3 TW,  
294 which is smaller than our combined heat transport of 4.8 TW (Figures S3 and S4).

#### 295 4.2 Transport losses and exchanges

296 Despite the splitting and re-combination of the WGCC on the shelf between OSNAP West  
297 and AR7W (Gou et al., 2021), there is no loss in the volume or freshwater transport between  
298 those two sections. The same is true for the WGC between these sections. Continuing north to  
299 the Cape Desolation section, there is little change in the total northward transport (Figure 4).  
300 However, offshore exchanges leads to the WGCC losing 0.07 Sv and 4.0 mSv of its volume and  
301 freshwater transports, respectively to the WGC. Given that Pacini and Pickart (2021) observe  
302 significant meandering of the WGC at OSNAP West, it is likely that those meanders are then  
303 damped, given the transport coherence to Cape Desolation.

304 The observational study by Myers et al. (2009) showed the most significant exchange from  
305 the WGC to the Labrador Sea interior occurs between Cape Desolation and Fylla Bank.  
306 Majumder et al. (2021) has also pointed out that the offshore transport from the coast to the  
307 interior Labrador Sea mainly occurs at  $61^\circ\text{N}$ - $62^\circ\text{N}$ . Irminger Rings are also formed and  
308 exchange waters offshore in this region (Katsman et al., 2004). Although we see such offshore  
309 exchange, the ability to see more details of the currents with the high-resolution models shows us  
310 that the situation in this region is more complex. Offshore exchange from the shelf, likely due to  
311 Ekman transport, reduces the WGCC volume transport by over 50% between the Cape

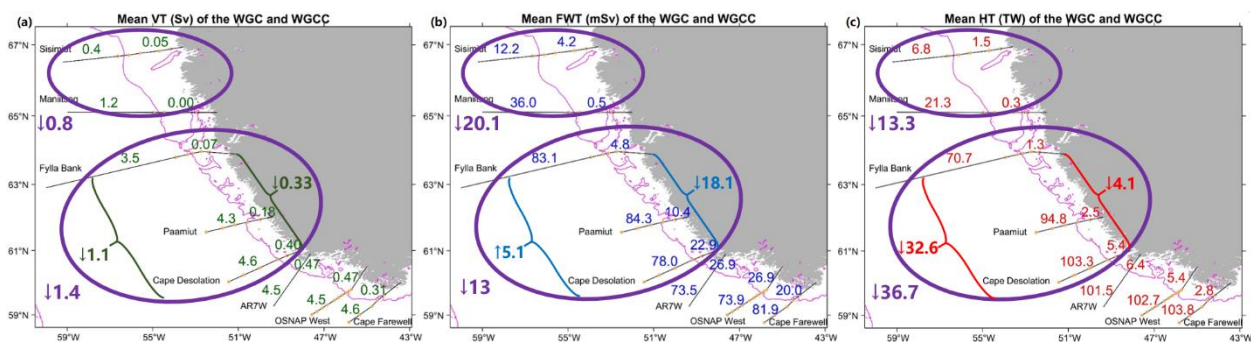
312 Desolation and Paamiut sections, with a further reduction to 0.07 Sv by the Fylla Bank section.  
 313 Similar reductions are seen (Figure 4). Similar losses are seen for the WGCC's freshwater and heat  
 314 transport.

315 Given the offshore losses by the WGCC are into the WGC, this additional waters masks  
 316 the offshore losses from the WGC (Figure 4). Although the volume transport of the WGC drops  
 317 only 0.3 Sv between the Cape Desolation and Paamiut sections, the total offshore exchange of  
 318 water between those same two sections is 0.5 Sv. Similarly the boundary current system loses a  
 319 total of 1.4 sv between the Cape Desolation and Fylla Bank sections. Interestingly, the WGC's  
 320 freshwater transport increases from the Cape Desolation to Paamiut sections, with only a small  
 321 drop through to the Fylla Bank section (Figure 4). However, given the significant losses from the  
 322 WGCC, in actual fact we seen a long term mean offshore freshwater transport of 13 mSv in this  
 323 region. The offshore exchange of heat is more consistent with the changes in the volume  
 324 transport, with 36.7 TW of heat fluxed into the interior of the Labrador Sea south of the Fylla  
 325 Bank section.

326 Myers et al. (2009) found warm season transports across the Fylla Bank section of 1.0 Sv  
 327 and 23.0 mSv. Yet, we find a long term mean transport of the WGC across the Fylla Bank  
 328 section of 3.5 Sv and 83.1 mSv (Figure 4). The reason for the difference is the extension of our  
 329 section in this analysis to catch the significant transport following the isobaths around the  
 330 northern rim of the Labrador Sea. Similarly, we find a WGC transport north across the  
 331 Maniitsoq section of 1.2 Sv while Myers et al. (2009) found close to zero. Again, our use of an  
 332 extended section captures transport continuing farther northward along the eastern margin of the  
 333 Labrador Sea before turning westward. The remaining 0.4 Sv we see at the Sisimiut section is  
 334 therefore the model's long term mean transport for the WGC into Baffin Bay, supplemented by  
 335 0.05 Sv by the WGCC on the shelf.

336 Similarly, for freshwater transport, the precipitous decreases seen in Myers et al (2009) for  
 337 the Fylla Bank and Maniitsoq sections compared to the Cape Desolation section are related to the  
 338 short length of the northern observational sections used, rather than a near complete exchange of  
 339 all the freshwater from the WGC into the interior of the Labrador Sea. Although there is little net  
 340 northward freshwater transport into Baffin Bay on the shelf, 12.2 mSv enter that basin via the  
 341 WGC. And the majority of the freshwater (over 80 mSv) carried north in the WGC, crosses the  
 342 Fylla Bank (and the Maniitsoq section for a significant fraction) before turning west and  
 343 circulating around the northern Labrador Sea. And although we don't look at exchange into the  
 344 Labrador Sea interior from its northern end, other studies (Schulze-Chretien and Frajka-Willians,  
 345 2018; Pennelly and Myers, 2019) find little such exchange in this northern region.

346

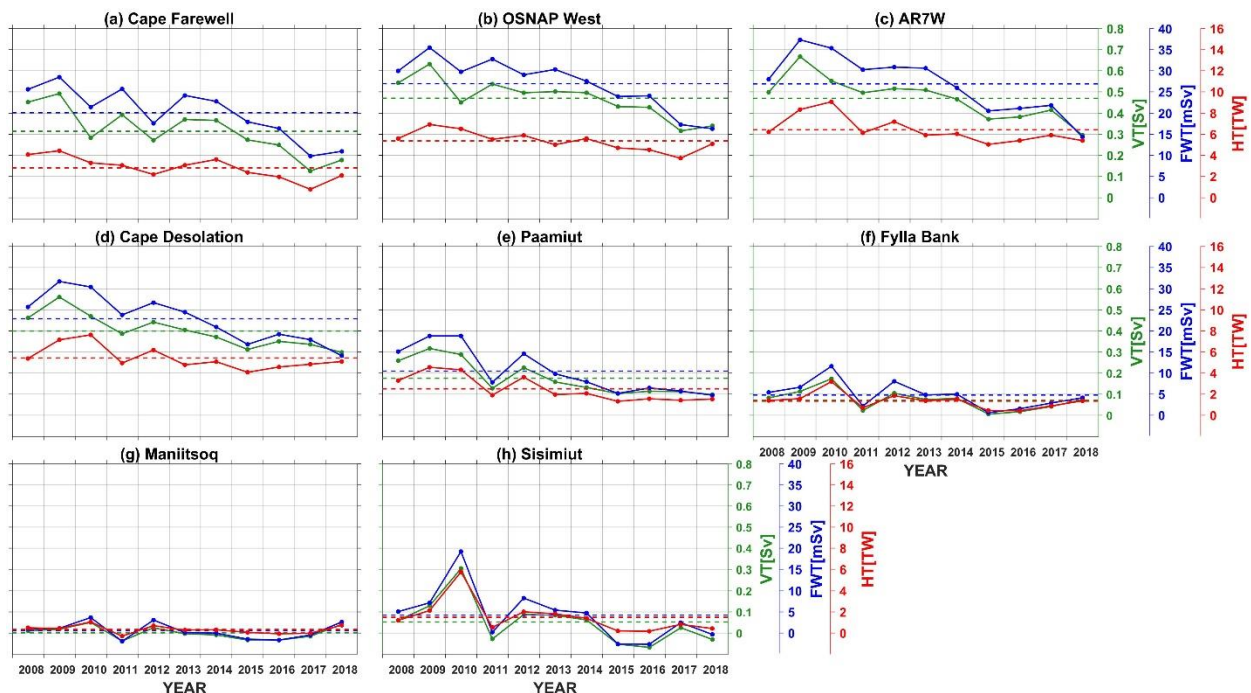


347 **Figure 4.** Schematic showing the annual means (2008-2018) of the volume transport (a),  
 348 freshwater transport (b), heat transport (c) for each section. The WGCC transports are denoted by  
 349 the numbers inshore of the 250 m isobath (magenta line), and the WGC transports are denoted by  
 350 the numbers offshore of the 250 m isobath. The transport losses of the WGCC and WGC from  
 351 Cape Desolation to Fylla Bank are labelled by offshore and onshore braces, respectively. The  
 352 total transport losses between sections are labelled by the purple circles and numbers.

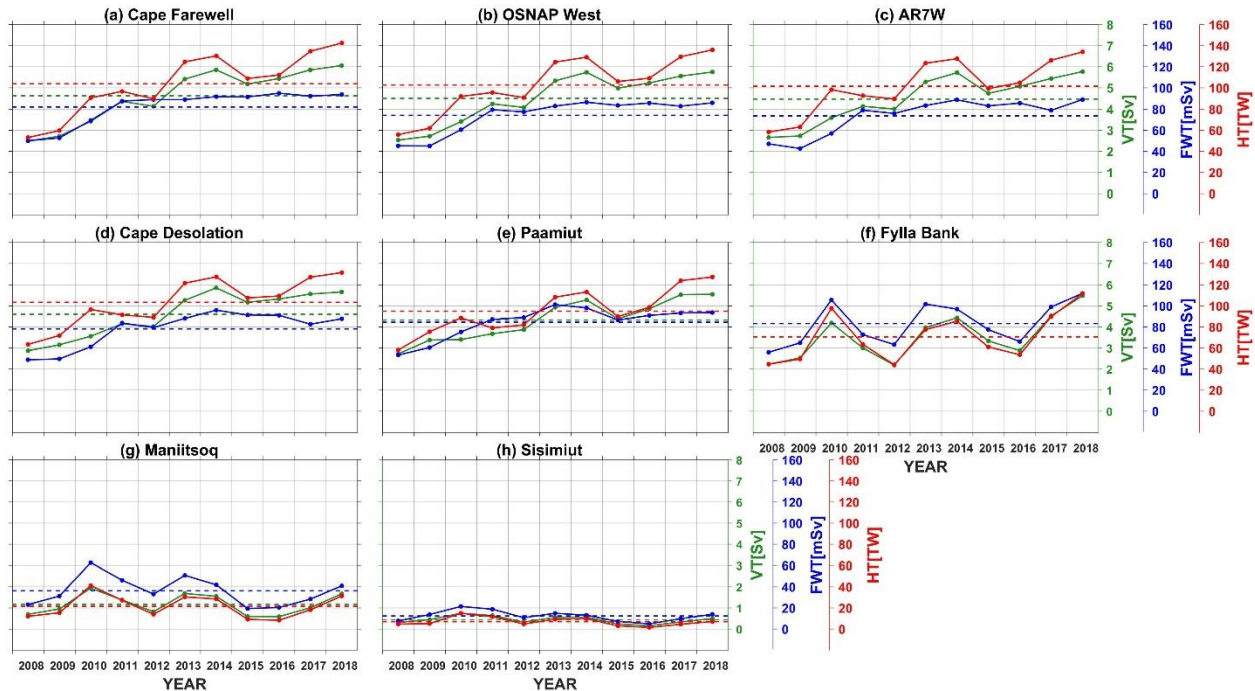
353 4.3 Inter-annual variability

354 Inter-annual events previously discussed are also reflected in the timeseries of the WGCC  
 355 (Figure 5) and WGC (Figure 6) transports. The WGCC transports at Sisimiut and WGC  
 356 transports at Maniitsoq are anomalously high in 2010, being  $\sim 0.3$  Sv and  $\sim 1$  Sv respectively  
 357 larger than the mean. Another peak of the WGCC freshwater transport at the northern three  
 358 sections is seen in 2012, while the WGC freshwater transports at these sections are minimal  
 359 values. 2012 is a year with record Greenland melt (Nghiem et al., 2012; Tedesco et al., 2013),  
 360 and the downwelling favorable winds during that year likely constrained the meltwater near the  
 361 coast and transported it northward to the Baffin Bay (Luo et al., 2016).

362 To the south of Fylla Bank, the trend of the WGC volume transport is opposite compared  
 363 to the WGCC, though the variations from year to year may not correspond perfectly. There is  
 364 unexpected southward WGCC transport of 0.05 Sv at Sisimiut and Maniitsoq in 2015 and 2016.  
 365 This is consistent with the assumption made by Rysgaard et al. (2020) based on an observational  
 366 water mass analysis, that southward coastal current transports exists in 2015 and 2016 south of  
 367 Davis Strait.



368  
 369 **Figure 5.** Annual WGCC transports with dashed lines denoting long-term means over 2008-  
 370 2018. Green, blue, red lines and y-axes correspond to volume transports (VT), freshwater  
 371 transports (FWT), heat transports (HT) respectively. Each of the sections are identified in Figure  
 372 1b.



373  
374 **Figure 6.** Same as Figure 2 but for the WGC.

375

## 376 5 The Forcing Mechanisms

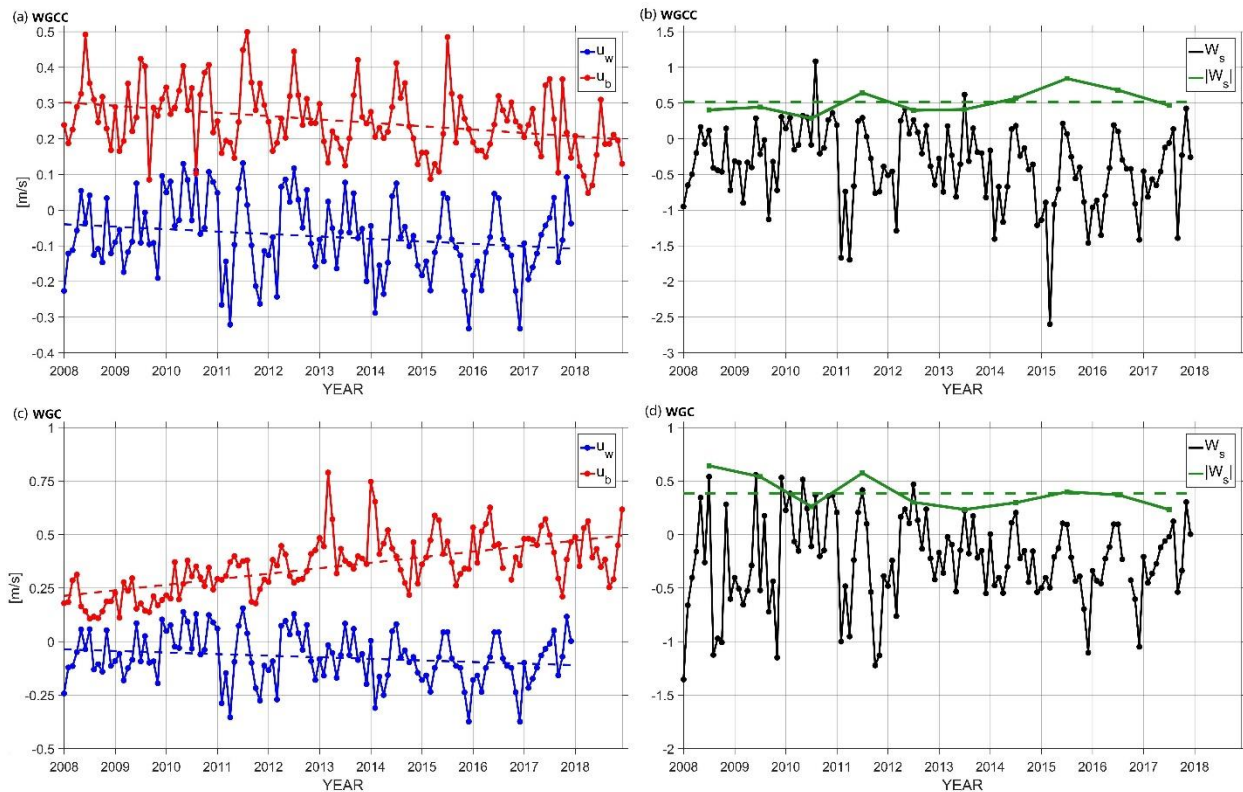
377 We now explore the forcing mechanisms of the currents and try explaining their inter-  
 378 annual variability. The monthly  $u_w$  and  $u_b$  of the WGCC at the Cape Desolation section are  
 379 shown in Figure 7a. As  $u_w$  is mostly negative throughout the ten-year period except in summer,  
 380 upwelling favorable winds should prevail in this region that counter the buoyancy-driven flow  
 381 (Whitney & Garvine, 2005). While during 2010 when  $u_w$  is mostly positive, downwelling  
 382 favorable winds prevail that augment the flow (Whitney & Garvine, 2005). This wind pattern  
 383 and its anomaly in 2010 corresponds to those indicated by Myers et al. (2021).

384 The decreasing trends of both the  $u_b$  and  $u_w$  could largely explain the decreasing trends of  
 385 the WGCC transports. As  $|W_s|$  is mostly  $<1$  throughout the whole period with a mean of  $\sim 0.5$   
 386 (Figure 7b), the WGCC is predominantly buoyancy driven. And when the wind is downwelling  
 387 favorable ( $W_s > 0$ ),  $|W_s|$  is mostly  $<0.5$ . While when the wind is upwelling favorable ( $W_s < 0$ ),  
 388 the frequency of events with  $|W_s| > 0.5$  or even  $|W_s| > 1$  is significantly more likely. Therefore, the  
 389 possibility of anomalously strong upwelling favorable winds is larger than that for the  
 390 downwelling favorable winds, thus having a larger impact on the WGCC overall.

391 Using shipboard data in summer 2014, Lin et al. (2018) evaluated the  $|W_s|$  for the coastal  
 392 current rounding Cape Farewell in the vicinity of the south Greenland, finding a mean of 0.18  
 393 and a range of 0.05-0.41. Sutherland & Pickart (2009) showed that the  $|W_s|$  for the EGCC at an  
 394 observational section just east of Cape Farewell, in the summers from 1997 to 2004, was in the  
 395 range of 0.02-0.5, although except for being 0.5 at Cape Farewell in summer 2003, the  $|W_s|$  was  
 396 below 0.25. They showed that the  $|W_s|$  for the EGCC at sections north of Cape Farewell in  
 397 summer 2004 in the range of 0.05-0.25. Our  $|W_s|$  of the WGCC in summer is generally lower  
 398 than that in other seasons (Figure 7b), so it is generally lower than the mean  $|W_s|$  and corresponds

399 well with these observational results, though there may be differences in wind and buoyancy  
 400 forcings between the west and east Greenland shelf. Note that Bacon et al. (2014)'s modelling  
 401 results showed that the  $|W_s|$  of the EGCC as close to 1 so that wind and buoyancy forcing were  
 402 similarly important to the EGCC.

403 In terms of the velocity components of the WGC at Cape Desolation (Figure 7c), its  $u_w$  is  
 404 basically the same as that of the WGCC (Figure 7a), as the wind does not change much over the  
 405 small spatial scale between shelf and shelfbreak current. Meanwhile  $u_b$  steadily increases over  
 406 2008-2018. The  $W_s$  of the WGC (Figure 4d) has similar features as that of the WGCC (Figure  
 407 7b), as indicated above, with a  $|W_s|$  of  $\sim 0.4$ . So the WGC at Cape Desolation is also  
 408 predominantly buoyancy driven. And the increasing trend of the  $u_b$  could largely explain the  
 409 trend of the WGC transports discussed above (Figure 3).



410

411 **Figure 7.** The monthly  $u_w$  (blue solid line) and  $u_b$  (red solid line) of the WGCC (a) and WGC (c)  
 412 at Cape Desolation, with dashed lines denoting their linear regressions. And the monthly  $W_s$   
 413 (black line) and its annual absolute value (green line) of the WGCC (b) and WGC (d) at Cape  
 414 Desolation, with the dashed green lines denoting the time-mean absolute values.

415

416 To the north of Cape Desolation, the forcing mechanisms of the currents change. The  $u_w$   
 417 term is similar among the sections, consistent with large atmospheric scales. But the buoyancy  
 418 terms evolve, changing the relative importance between wind and buoyancy forcing. At Fylla  
 419 Bank, as the frequency of  $|W_s| > 1$  and that of  $|W_s| < 1$  are both high (Figure S6b and S6d), wind  
 420 forcing and buoyancy forcing both become important to the WGCC and WGC, though the  
 421 frequency of  $|W_s| < 1$  for the WGCC is much larger before 2009. Similarly, at Sisimiut, wind  
 422 forcing and buoyancy forcing are both important to the WGCC (Figure S7b), while the wind

423 forcing is dominant in forcing the WGC as  $|W_s|$  is mostly  $>1$  (Figure S7d). In all cases indicated  
424 in this paragraph, the time-mean  $|W_s|$  is much larger than 1, since extremely large  $|W_s|$  exists  
425 sometimes, especially when  $W_s < 0$ .

## 426 **6 Discussion and Conclusions**

427 Using ten-years of output from a high-resolution ( $1/60^\circ$ ) numerical model, we presented  
428 the inter-annual variability of the WGC and WGCC in terms of their speeds, transports and  
429 forcing mechanisms. The WGCC and WGC are found to extend to Davis Strait during most  
430 years, especially during 2010 when the current speeds and transports are the highest in the study  
431 period. This could be due to the anomalous wind pattern in 2010 (Myers et al., 2021). The  
432 freshwater transports of the WGCC at the northern three sections showed maximums in 2012,  
433 which could be the result of the record Greenland melt and downwelling favorable winds in that  
434 year (Nghiem et al., 2012; Tedesco et al., 2013; Luo et al., 2016). While in 2015 and 2016, the  
435 transports of the WGCC at Sisimiut and Maniitsoq are southward, consistent with the assumption  
436 made by Rysgaard et al. (2020). And at southwest Greenland, the inter-annual trends of the  
437 speeds and transports of the WGCC are opposite to those of the WGC, with the WGCC declining  
438 and the WGC strengthening, over 2008-2018.

439 At Cape Desolation where large Greenland runoff exists, the WGCC and WGC are both  
440 predominantly buoyancy forced, and their buoyancy forced velocity components largely explains  
441 their transport variability. At Fylla Bank and Sisimiut, the wind forcing is more dominant, and  
442 the WGCC and WGC are forced by both wind and buoyancy except that the WGC at Sisimiut is  
443 predominantly wind forced. Generally, upwelling favorable winds provide a stronger forcing  
444 than downwelling favorable winds.

445 Since both the WGC and WGCC are predominantly buoyancy-forced at Cape Desolation,  
446 their opposite trends in inter-annual variability implies the opposite impacts from Greenland and  
447 Arctic melt on the currents, which could change horizontal density gradients across the currents  
448 and thus their  $u_b$ . There are areas like Juliannehaab Bight in the southwest Greenland (Figure 1a)  
449 that have significant Greenland melt discharge. And the WGC and the WGCC are the extensions  
450 of the East Greenland Current and EGCC, which originate from Fram Strait where large Arctic  
451 outflows pass through (Bacon et al., 2014; Sutherland & Pickart, 2009). In terms of the  
452 Greenland melt, the model experiment by Dukhovskoy et al., (2019) has shown a considerable  
453 lateral advection of the Greenland melt from the southwest Greenland shelf to the interior  
454 Labrador Sea. It was also suggested that the Greenland melt would be intensively vertically  
455 mixed as crossing the shelf.

456 The transport decrease along the coast suggests substantial exchanges from the current  
457 system into the interior and northern Labrador Sea region. And the main exchange into the  
458 interior occurs between Cape Desolation and Fylla Bank, with the WGCC being the main  
459 freshwater source. The density anomalies in the Labrador Sea are mainly thought to be  
460 originated from the eastern subpolar gyre (Li et al., 2021), however, the exchange into the  
461 interior Labrador Sea also could generate density anomalies. The freshwater and heat inflows of  
462 13 mSv and 36.7 TW from the current system play nonnegligible roles in setting the  
463 preconditioning and restratification of the deep convection. Yet, as we show, the majority of the  
464 freshwater ( $\sim 87\%$ ) and heat ( $\sim 66\%$ ) in the combined WGC/WGCC current system are  
465 transported into the northern part of the basin, past the Fylla Bank section (Fig. 4), where they  
466 likely circulate around the basin, before flowing south with the Labrador Current. This is also

467 consistent with tracer and virtual Lagrangian float studies that show most of the freshwater  
468 coming from the Greenland icesheet reaches the northern Labrador Sea and/or the Labrador  
469 current rather than the interior convective patch (Gillard et al., 2016, Luo et al., 2016). This may  
470 be why higher resolution model studies generally do not find a significant impact of Greenland  
471 freshwater on Labrador Sea water formation as of yet (e.g. Böning et al., 2016). Poor  
472 representation of the WGCC and shelf processes may lead to low salinity water being farther  
473 offshore in coarse resolution models and thus easier to exchange into the interior. For example,  
474 based on a 1/12th degree simulation functionally equivalent to the intermediate nest used here,  
475 Pennelly and Myers (2019) found a long-term (2006–2016) annual mean exchange of  $21 \pm 11$   
476 mSv of freshwater (also relative to 34.8) across the 2,000-m isobath to the interior of the  
477 Labrador Sea. Which is almost double our estimate of 13 mSv over 2008-2018, which is unlikely  
478 to be due to the small difference in averaging period.

479 Limited exchange of freshwater into the Labrador Sea interior is also consistent with  
480 strong deep convection occurring in the Labrador Sea in recent winters (Yashayaev and Loder,  
481 2016). Thus, even if a warming climate leads to continued enhancement in Greenland and Arctic  
482 melt and an increase in transport in the WGC system, it is open question if a significant  
483 component of that increase will reach the convective portion of the interior of the Labrador Sea.  
484 It is possible such additional low salinity water may accumulate in Baffin Bay, although  
485 Dukhovskoy et al. (2021) suggests that the sub-polar interior will be more sensitive to enhanced  
486 freshwater from the southwest Greenland shelf. If much of the recent increases in Greenland  
487 melt (Bamber et al., 2018) was not lost to the interior of the Labrador Sea, but followed the  
488 boundary current system around the Labrador Sea, there is potential that this water contributed to  
489 the record sub-polar gyre freshening event between 2012 and 2016 that Holliday et al. (2020)  
490 reported on.

## 491 **Acknowledgments**

492 The authors declare no competing financial interests. This work was funded by Natural Sciences  
493 and Engineering Research Council of Canada (NSERC) grants awarded to PGM. These include  
494 Discovery Grants (rgpin 227438-09 and 2020-04344) and a Climate Change and Atmospheric  
495 Research Grant (433898). GLORYS reanalysis received support from Mercator Ocean, Groupe  
496 Mission Mercator Coriolis and the European Community's Seventh Framework Programme  
497 FP7/2007-2013 under Grant Agreement number 218812 (MyOcean). The authors would like to  
498 thank the NEMO development team as well as the DRAKKAR group for providing the model  
499 code and continuous guidance.

500 The Fortran code used to carry out the LAB60 simulation can be accessed from the  
501 NEMO version 3.6 repository  
502 (<https://forge.ipsl.jussieu.fr/nemo/browser/NEMO/releases/release-3.6>), last access: 14 October  
503 2020). A few Fortran files were modified to handle our passive tracers. The complete Fortran  
504 files as well as the CPP keys, namelists, and associated files can be found on Zenodo  
505 (<https://doi.org/10.5281/zenodo.3762748>, Pennelly, 2020). Due to the large storage demands for  
506 a 1/60 degree resolution simulation with daily output that spans 14 years, the initial and  
507 boundary conditions, atmospheric forcing, and numerical output remains on the high  
508 performance computing platform Compute Canada. We express our thanks to Compute Canada  
509 (<http://www.computeCanada.ca>) for the computational resources to carry out our numerical  
510 simulations as well as archival of the experiments.

511 **References**

- 512 Azetsu-Scott, K., Petrie, B., Yeats, P. & Lee, C. (2012). Composition and fluxes of freshwater  
513 through Davis Strait using multiple chemical tracers, *Journal of Geophysical Research: Oceans*,  
514 *117*, C12011. doi:10.1029/2012JC008172.
- 515 Bacon, S., Marshall, A., Holliday, N. P., Aksenov, Y., & Dye, S. R. (2014). Seasonal variability  
516 of the East Greenland Coastal Current. *Journal of Geophysical Research: Oceans*, *119*(6), 3967–  
517 3987. doi:10.1002/2013JC009279
- 518 Bamber, J. L., Tedstone, A. J., King, M. D., Howat, I. M., Enderlin, E. M., van den Broeke, M.  
519 R., & Noel, B. (2018). Land ice freshwater budget of the Arctic and North Atlantic Oceans: 1.  
520 Data, methods, and results. *Journal of Geophysical Research: Oceans*, *123*, 1827–1837.  
521 doi:10.1002/2017JC013605
- 522 Böning, C. W., Behrens, E., Biastoch, A., Getzlaff, K., & Bamber, J. L. (2016). Emerging impact  
523 of Greenland meltwater on deepwater formation in the North Atlantic Ocean. *Nature*  
524 *Geoscience*, *9*(7), 523-527.
- 525 Bracco, A., Pedlosky, J., & Pickart, R. S. (2008). Eddy formation near the west coast of  
526 Greenland. *Journal of Physical Oceanography*, *38*(9), 1992–2002. doi:10.1175/2008JPO3669.1
- 527 Castelao, R. M., Luo, H., Oliver, H., Rennermalm, A. K., Tedesco, M., & Bracco, A., et al  
528 (2019). Controls on the transport of meltwater from the southern Greenland ice sheet in the  
529 Labrador Sea. *Journal of Geophysical Research: Oceans*, *124*, 3551–3560.  
530 doi:10.1029/2019JC015159
- 531 Castro de la Guardia, L., Hu, X., & Myers, P. G. (2015). Potential positive feedback between  
532 Greenland Ice Sheet melt and Baffin Bay heat content on the west Greenland shelf. *Geophysical*  
533 *Research Letters*, *42*, 4922–4930. doi:10.1002/2015GL064626.
- 534 Cuny, J., Rhines, P. B., & Kwok, R (2005). Davis Strait volume, freshwater and heat fluxes.  
535 *Deep Sea Research Part I: Oceanographic Research Papers*, *52*(3), 519-542.  
536 doi:10.1016/j.dsr.2004.10.006.
- 537 Curry, B., Lee, C. M., & Petrie, B. (2011). Volume, Freshwater, and Heat Fluxes through Davis  
538 Strait, 2004–05, *Journal of Physical Oceanography*, *41*(3), 429-436.  
539 doi:10.1175/2010JPO4536.1
- 540 Curry, B., Lee, C. M., Petrie, B., Moritz, R. E., & Kwok, R. (2014). Multiyear Volume, Liquid  
541 Freshwater, and Sea Ice Transports through Davis Strait, 2004–10, *Journal of Physical*  
542 *Oceanography*, *44*(4), 1244-1266. doi:10.1175/JPO-D-13-0177.1
- 543 de Jong, M. F., Bower, A. S., & Furey, H. H. (2014). Two years of observations of warm-core  
544 anticyclones in the Labrador Sea and their seasonal cycle in heat and salt stratification. *Journal*  
545 *of Physical Oceanography*, *44*(2), 427–444. doi: 10.1175/JPO-D-13-070.1
- 546 Dukhovskoy, D. S., Myers, P. G., Platov, G., Timmermans, M. L., Curry, B., Proshutinsky, A., et  
547 al. (2016). Greenland freshwater pathways in the sub-Arctic Seas from model experiments with  
548 passive tracers. *Journal of Geophysical Research: Oceans*, *121*(1), 877–907.  
549 doi:10.1002/2015jc011290

- 550 Dukhovskoy, D. S., Yashayaev, I., Chassignet, E. P., Myers, P. G., Platov, G., & Proshutinsky,  
551 A. (2021). Time Scales of the Greenland Freshwater Anomaly in the Subpolar North Atlantic.  
552 *Journal of Climate*, 34(22), 8971–8987. doi:10.1175/JCLI-D-20-0610.1.
- 553 Dukhovskoy, D. S., Yashayaev, I., Proshutinsky, A., Bamber, J. L., Bashmachnikov, I. L.,  
554 Chassignet, E. P., et al. (2019). Role of Greenland freshwater anomaly in the recent freshening of  
555 the subpolar North Atlantic. *Journal of Geophysical Research: Oceans*, 124(5), 3333–3360.  
556 doi:10.1029/2018JC014686
- 557 Dussin, R., Barnier, B., & Brodeau, L. (2016). *The making of Drakkar Forcing Set DFS5*.  
558 Grenoble, France: LGGE.
- 559 Duyck, E., & De Jong, M. F. (2021). Circulation over the South-East Greenland shelf and  
560 potential for liquid freshwater export: A drifter study. *Geophysical Research Letters*, 48,  
561 e2020JB020886. doi.:10.1029/2020GL091948
- 562 Gillard, L. C., Hu, X., Myers, P. G., & Bamber, J. L. (2016). Meltwater pathways from marine  
563 terminating glaciers of the Greenland ice sheet. *Geophysical Research Letters*, 43(20), 10873–  
564 10882. doi:10.1002/2016GL070969
- 565 Gou, R., Feucher, C., Pennelly, C., & Myers, P. G. (2021). Seasonal cycle of the coastal west  
566 Greenland current system between Cape Farewell and Cape Desolation from a very high-  
567 resolution numerical model. *Journal of Geophysical Research: Oceans*, 126, e2020JC017017.  
568 doi.:10.1029/2020JC017017
- 569 Hall, M. M., Torres, D. J., & Yashayaev, I. (2013). Absolute velocity along the AR7W section in  
570 the Labrador Sea. *Deep Sea Research Part I: Oceanographic Research Papers*, 72, 72–87.  
571 doi:10.1016/j.dsr.2012.11.005
- 572 Holliday, N. P., Bersch, M., Berx, B., Chafik, L., Cunningham, S., & Florindo-López, C., et al.  
573 (2020). Ocean circulation causes the largest freshening event for 120 years in eastern subpolar  
574 North Atlantic. *Nature communications*, 11, 585. doi: 10.1038/s41467-020-14474-y.
- 575 Hu, X., Sun, J., Chan, T.O., & Myers, P. G. (2018). Thermodynamic and Dynamic Ice Thickness  
576 Contributions in the Canadian Arctic Archipelago in NEMO-LIM2 Numerical Simulations. *The  
577 Cryosphere*, 12(4), 1233–1247. doi:10.5194/tc-12-1233-2018
- 578 Jackson, L. C., Peterson, K. A., Roberts, C. D., & Wood, R. A. (2016). Recent slowing of  
579 Atlantic overturning circulation as a recovery from earlier strengthening. *Nature Geoscience*, 9,  
580 518–522. doi:10.1038/ngeo2715
- 581 Katsman, C. A., Spall, M. A., & Pickart, R. S. (2004). Boundary current eddies and their role in  
582 the restratification of the Labrador Sea. *Journal of Physical Oceanography*, 34(9), 1967–1983.  
583 doi:10.1175/1520-0485(2004)0342.0.CO;2
- 584 Le Bras, I. A. A., Straneo, F., Holte, J., & Holliday, N. P. (2018). Seasonality of freshwater in  
585 the East Greenland Current system from 2014 to 2016. *Journal of Geophysical Research:  
586 Oceans*, 123(12), 8828–8848. doi:10.1029/2018JC014511
- 587 Li, F., Lozier, M. S., Bacon, S., Bower, A. S., Cunningham, S. A., & De Jong M. F., et al.  
588 (2021). Subpolar North Atlantic western boundary density anomalies and the Meridional  
589 Overturning Circulation. *Nature Communications*, 12(1), 3002. doi: 10.1038/s41467-021-23350-  
590 2

- 591 Lin, P., Pickart, R. S., Torres, D. J., & Pacini, A. (2018). Evolution of the Freshwater Coastal  
592 Current at the Southern Tip of Greenland. *Journal of Physical Oceanography*, 48(9), 2127-2140.  
593 doi:10.1175/JPO-D-18-0035.1
- 594 Lique, C., Treguier, A. M., Scheinert, M., & Penduff, T. (2009). A model-based study of ice and  
595 freshwater transport variability along both sides of Greenland. *Climate Dynamics*, 33, 685–705.  
596 doi:10.1007/s00382-008-0510-7
- 597 Lozier, M. S., Bacon, S., Bower, A. S., Cunningham, S. A., de Jong, M. F., de Steur, L., et al.  
598 (2017). Overturning in the Subpolar North Atlantic Program: A new international ocean  
599 observing system. *Bulletin of the American Meteorological Society*, 98, 737–752.  
600 doi:10.1175/BAMS-D-16-0057.1
- 601 Luo, H., Castelao, R. M., Rennermalm, A. K., Tedesco, M., Bracco, A., Yager, P., et al. (2016).  
602 Oceanic transport of surface meltwater from the southern Greenland ice sheet. *Nature*  
603 *Geoscience*, 9(7), 528-532. doi:10.1038/ngeo2708
- 604 Madec, G (2008). *Nemo ocean engine, Note du Pôle de modélisation*, 27. France: Institut Pierre-  
605 Simon Laplace (IPSL).
- 606 Mortensen, J. (2018). *Report on hydrographic conditions off Southwest Greenland June/July*  
607 *2017*. NAFO SCR Doc 18/005, Serial No. N6782.
- 608 Majumder, S., Castelao, R. M., & Amos, C. M. (2021). Freshwater variability and transport in  
609 the Labrador Sea from in situ and satellite observations. *Journal of Geophysical Research:*  
610 *Oceans*, 126, e2020JC016751. doi:10.1029/2020JC016751
- 611 Myers, P. G., Castro de la Guardia, L., Fu, C., Gillard, L. C., Grivault, N., Hu, X., et al. (2021).  
612 Extreme high Greenland Blocking Index leads to the reversal of Davis and Nares Strait net  
613 transport toward the Arctic Ocean. *Geophysical Research Letters*, 48, e2021GL094178.  
614 doi:10.1029/2021GL094178
- 615 Myers, P. G., Donnelly, C., & Ribergaard, M. H. (2009). Structure and variability of the West  
616 Greenland Current in summer derived from 6 repeat standard sections. *Progress in*  
617 *Oceanography*, 80(1–2), 93–112. doi:10.1016/j.pocean.2008.12.003
- 618 Myers, P. G., Kulan, N., & Ribergaard, M. H. (2007). Irminger Water variability in the West  
619 Greenland Current. *Geophysical Research Letters*, 34(17), 217-239. doi:10.1029/2007GL030419
- 620 Nghiem, S. V., Hall, D. K., Mote, T. L., Tedesco, M., Albert, M. R., & Keegan, K., et al. (2012).  
621 The extreme melt across the Greenland ice sheet in 2012. *Geophysical Research Letters*, 39,  
622 L20502. doi:10.1029/2012GL053611
- 623 Pacini, A., & Pickart, R. S. (2021). Meanders of the West Greenland Current near Cape  
624 Farewell. *Deep Sea Research Part I: Oceanographic Research Papers*, 179, 103664.  
625 doi:10.1016/j.dsr.2021.103664
- 626 Pacini, A., Pickart, R.S., Bahr, F., Torres, D.J., Ramsey, A.L., & Holte, J. (2020). Mean  
627 conditions and seasonality of the West Greenland Boundary Current System near Cape Farewell.  
628 *Journal of Physical Oceanography*. 50(10), 2849–2871, doi:10.1175/JPO-D-20-0086.1
- 629 Pennelly, C., Hu, X., & Myers, P. G.(2019). Cross-isobath freshwater exchange within the North  
630 Atlantic subpolar gyre. *Journal of Geophysical Research: Oceans*, 124, 6831-6853.  
631 doi:10.1029/2019JC015144

- 632 Pennelly, C. & Myers, P. G. (2020). Introducing LAB60: A 1/60° NEMO 3.6 numerical  
633 simulation of the Labrador Sea. *Geoscientific Model Development*, 13, 4959–4975,  
634 doi:10.5194/gmd-2020-111
- 635 Pennelly, C., & Myers, P. G. (2021). Impact of different atmospheric forcing sets on modeling  
636 Labrador Sea Water production. *Journal of Geophysical Research: Oceans*, 126,  
637 e2020JC016452. doi:10.1029/2020JC016452
- 638 Rykova, T., Straneo, F., & Bower, A. S. (2015). Seasonal and interannual variability of the West  
639 Greenland Current System in the Labrador Sea in 1993-2008. *Journal of Geophysical Research:*  
640 *Oceans*, 120(2), 1318-1332. doi:10.1002/2014jc010386
- 641 Rysgaard, S., Boone, W., Carlson, D., Sejr, M. K., Bendtsen, J., & Juul-Pedersen, T., et al.  
642 (2020). An updated view on water masses on the pan-west Greenland continental shelf and their  
643 link to proglacial fjords. *Journal of Geophysical Research: Oceans*, 125, e2019JC015564.  
644 doi:10.1029/2019JC015564
- 645 Schulze-Chretien, L. M., & Frajka-Williams, E. (2018). Wind-driven transport of fresh shelf  
646 water into the upper 30 m of the Labrador Sea. *Ocean Science*, 14(5), 1247-1264.  
647 doi:10.5194/os-14-1247-2018
- 648 Smith, G. C., Roy, F., Mann, P., Dupont, F., Brasnett, B., Lemieux, J.-F., et al. (2014). A new  
649 atmospheric dataset for forcing ice-ocean models: Evaluation of reforecasts using the Canadian  
650 global deterministic prediction system. *Quarterly Journal of the Royal Meteorological Society*,  
651 140(680), 881–894. doi:10.1002/qj.2194
- 652 Stein, M. (2004). Climatic overview of NAFO Subarea 1 1991–2000. *Journal of Northwest*  
653 *Atlantic Fishery Science*, 34, 29–40. doi:10.2960/J.v34.m474
- 654 Sutherland, D. A., & Pickart, R. S. (2008). The East Greenland Coastal Current: Structure,  
655 variability, and forcing. *Progress in Oceanography*, 78 (1), 58-77.  
656 doi:10.1016/j.pocean.2007.09.006
- 657 Tedesco, M., Fettweis, X., Mote, T., Wahr, J., Alexander, P., Box, J. E., & Wouters, B. (2013).  
658 Evidence and analysis of 2012 Greenland records from spaceborne observations, a regional  
659 climate model and reanalysis data. *The Cryosphere*, 7, 615–630. doi:10.5194/tc-7-615-2013
- 660 Thornalley, D. J. R., Oppo, D. W., Ortega, P., Robson, J. I., Brierley, C. M., & Davis, R., et al.  
661 (2018). Anomalously weak Labrador Sea convection and Atlantic overturning during the past  
662 150 years. *Nature*, 556, 227–230. doi:10.1038/s41586-018-0007-4
- 663 Whitney, M. M., & Garvine, R. W. (2005). Wind influence on a coastal buoyant outflow,  
664 *Journal of Geophysical Research*, 110, C03014. doi:10.1029/2003JC002261
- 665 Yashayaev, I., & Loder, J. W. (2017). Further intensification of deep convection in the Labrador  
666 Sea in 2016. *Geophysical Research Letters*, 44, 1429–1438. doi:10.1002/2016GL071668.
- 667 Zou, S., Lozier, M. S., Li, F., Abernathey, R., & Jackson, L. (2020). Density-compensated  
668 overturning in the Labrador Sea. *Nature Geoscience*, 13, 121–126. doi: 10.1038/s41561-019-  
669 0517-1